

GeMuCo: Generalized Multisensory Correlational Model for Body Schema Learning

Kento Kawaharazuka¹, Kei Okada¹, and Masayuki Inaba¹

Abstract—Humans can autonomously learn the relationship between sensation and motion in their own bodies, estimate and control their own body states, and move while continuously adapting to the current environment. On the other hand, current robots control their bodies by learning the network structure described by humans from their experiences, making certain assumptions on the relationship between sensors and actuators. In addition, the network model does not adapt to changes in the robot’s body, the tools that are grasped, or the environment, and there is no unified theory, not only for control but also for state estimation, anomaly detection, simulation, and so on. In this study, we propose a Generalized Multisensory Correlational Model (GeMuCo), in which the robot itself acquires a body schema describing the correlation between sensors and actuators from its own experience, including model structures such as network input/output. The robot adapts to the current environment by updating this body schema model online, estimates and controls its body state, and even performs anomaly detection and simulation. We demonstrate the effectiveness of this method by applying it to tool-use considering changes in grasping state for an axis-driven robot, to joint-muscle mapping learning for a musculoskeletal robot, and to full-body tool manipulation for a low-rigidity plastic-made humanoid.

I. INTRODUCTION

Humans can continuously estimate and control their physical state by autonomously learning the relationship between various sensations and movements of their body, allowing them to adapt to the current environment and keep moving. A human can compensate for the lack of some their senses by using various other senses, just as a blindfolded human can roughly determine the position of their hand or a grasped tool from their own proprioception. Even in a complex body structure with joints, muscles, and tendons, the body gradually learns how to move by constantly learning the correlation between sensation and motion in an autonomous manner. Even if the body changes over time, or if the tools to be manipulated or the state of grasping changes, a human can detect and adapt to these changes, and can always estimate and control the state of the body appropriately. In this study, this human function is expressed in terms of a body schema, which represents the relationship between various sensors and actuators considering the body structure [1], [2]. We have considered the following four requirements that a body schema should have in an intelligent robot system (Fig. 1).

- **Multisensory Correlation** - capable of expressing correlation among various sensors and actuators

¹ The authors are with the Department of Mechano-Informatics, Graduate School of Information Science and Technology, The University of Tokyo, 7-3-1 Hongo, Bunkyo-ku, Tokyo, 113-8656, Japan. [kawaharazuka, k-okada, inaba]@jsk.t.u-tokyo.ac.jp

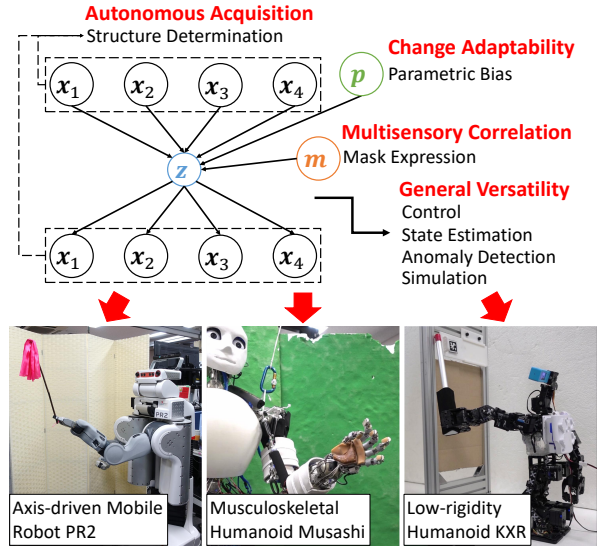


Fig. 1. The concept of this study. Generalized Multisensory Correlational Model (GeMuCo) has four characteristics: Multisensory Correlation, General Versatility, Autonomous Acquisition, and Change Adaptability. This body schema model is used for motion control, state estimation, anomaly detection, and simulation of robots with various configurations.

- **General Versatility** - can be used to construct basic components from control to state estimation, anomaly detection, and simulation
- **Autonomous Acquisition** - enables acquisition of models, including network structures, through autonomous learning
- **Change Adaptability** - capable of coping with gradual changes in body schema by updating the model online

Note that **Multisensory Correlation** and **Change Adaptability** come from the fundamental features of body schema outlined in [1], specifically termed as “Adaptable” and “Supramodel.” Also, **General Versatility** comes from the perspective of applying the definition of body schema to robots, while **Autonomous Acquisition** comes from the context of the human process of acquiring the body schema.

In the following, we discuss previous research related to these four requirements and the body schema itself, and our contributions.

A. Multisensory Correlation

Multisensory Correlation is not simply a matter of dealing with multiple sensors. It is necessary to express correlations among various sensors so that the model can cope with situations such as when a certain sensor is unavailable, or when a certain control input is not desired to

be used. On the other hand, most of existing methods use proprioception, visual, tactile, and other sensors as network inputs at one time for end-to-end processing [3]–[5], and there is limited research directly addressing correlations of multiple modalities.

B. General Versatility

For **General Versatility**, previous learning methods have generally been structured to achieve one goal, e.g. motion control [6], recognition [7], and anomaly detection [8]. On the other hand, there are few examples of integrating these multiple tasks in a single network. If control, state estimation, anomaly detection, simulation, etc. can be handled in a unified manner using a general-purpose computation procedure based on a single model, the learning results can be uniformly reflected in these components, and manageability can be improved.

C. Autonomous Acquisition

For **Autonomous Acquisition**, it is important not to use manually constructed assumptions for each robot, no matter how complex the body structure is. Although various learning-based control methods have been developed for complex robots such as those with flexible links [9], these methods make many assumptions on the structure of the problem and cannot be used for musculoskeletal structures, flexible tools, flexible objects, etc. in a unified manner. While there have been many attempts using imitation learning [10] and reinforcement learning [11], there are limited methods that allow actual robots to learn from experience without human intervention. Also, autonomous acquisition should not be limited to the mere acquisition of a model through learning. For truly autonomous acquisition, it is necessary for a robot to acquire even the structure of the model itself autonomously. Although the most common network structure determination method is Neural Architecture Search (NAS) for deep neural networks [12], these are parameter searches of neural networks, and the input/output of the network is generally fixed. Note that some methods utilizing mutual information and self-organizing maps have also been developed [13], [14].

D. Change Adaptability

For **Change Adaptability**, existing methods rarely incorporate information about gradual model changes directly into the models [15], [16]. In reinforcement learning [3] and supervised learning [6], adaptive behavior is generated by collecting a large amount of data in various environments. In other words, if the purpose of the behavior is uniquely determined, adaptive behavior can be produced by collecting data in various environmental conditions. On the other hand, if the purpose of the behavior is not uniquely determined and the model is to be used for various control, state estimation, anomaly detection, etc., it is difficult to obtain the change adaptability by simply inputting a large amount of data into the network.

E. Body Schema in Robotics

Research on body schema learning in robotics has been conducted extensively [2], [17]. The simplest example of body schema would be a generic robot model. Efforts to identify models with parameters such as link length, weight, and inertia have been numerous [18]. However, these efforts are limited to easily modelable robots and cannot handle **Multisensory Correlation**. There have also been attempts at body schema learning in more challenging setups, such as when the link structure is unknown [19], but these still make numerous assumptions about the robot’s body structure. Recently, body schema learning methods using deep learning have been developed to overcome these limitations [5], but the network structure is human-designed and lacks **Autonomous Acquisition** and **Change Adaptability**. Conversely, methods that heavily address **Change Adaptability** often lack **Multisensory Correlation** and **General Versatility** [15], [16]. Furthermore, alongside the recent development of foundational models, models that learn manipulation strategies end-to-end based on diverse sensory and linguistic inputs have emerged [20]. However, due to these models being very large and learning policies directly from teaching data, they lack **General Versatility**, **Autonomous Acquisition**, and **Change Adaptability**.

F. Our Contributions

From the above discussion, a body schema learning method that satisfies all the four requirements does not exist. Therefore, the purpose of this study is to improve the robot’s adaptive ability by modeling a body schema with these characteristics and having it learn autonomously. Drawing on our experiments which include tool-tip manipulation learning considering grasping state changes of axis-driven robots [21], joint-muscle mapping learning for musculoskeletal humanoid robots [22], and whole-body tool manipulation learning for low-rigidity humanoid robots [23], we propose a theoretical framework that consolidates these, called the Generalized Multisensory Correlation Model (GeMuCo). In this model, when the values of sensors and actuators are collectively represented by the variable x , the network structure is $(x, m) \rightarrow x$, using the mask variable m to represent the correlation between various sensors and actuators. This is a static body schema for static motions, i.e. motions for which there is a one-to-one correspondence between a certain control input and a sensation. Note that, in the case of dynamic motions, the network structure becomes a time-evolving dynamic body schema with different times at the input and output of the network [24]. In this study, we mainly discuss static body schema. Our contributions of GeMuCo are as follows:

- Multisensory correlation modeling by mask expression
- Versatile realization of control, state estimation, simulation, and anomaly detection by a single network
- Automatic acquisition of model structure including model input/output and their correlation
- Change adaptability by a mechanism of parametric bias

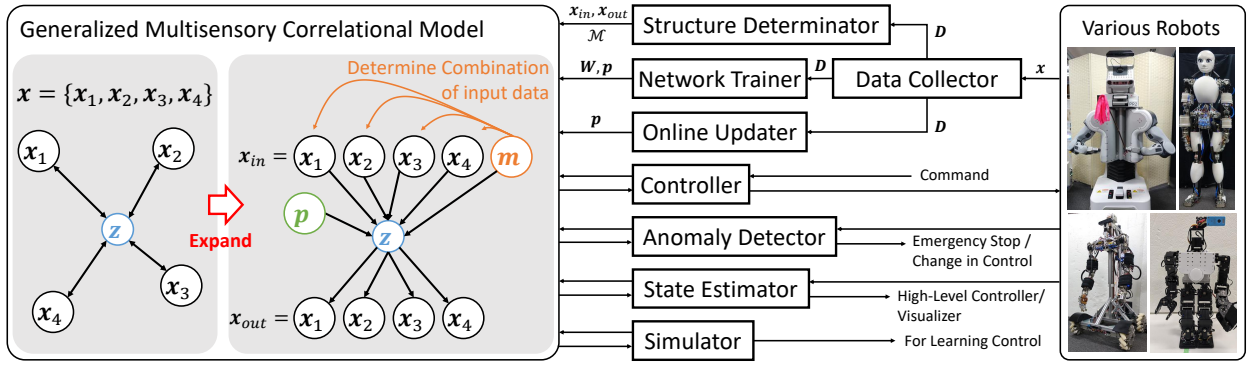


Fig. 2. System overview of GeMuCo with various basic components of Data Collector, Structure Determinator, Network Trainer, Online Updater, Controller, Anomaly Detector, State Estimator, and Simulator.

We hope that this study will contribute to the development of robots with autonomous learning capabilities similar to humans.

II. GEMUCO: GENERALIZED MULTISENSORY CORRELATIONAL MODEL

The overall system of Generalized Multisensory Correlational Model (GeMuCo) is shown in Fig. 2. First, various sensory and control input data are collected (Data Collector), and GeMuCo is trained based on these data (Network Trainer). In this process, the input/output of the network and the feasible mask set can be automatically determined from the data (Structure Determinator). During operation, GeMuCo always collects sensory and control input data and continuously updates part or all of it based on these data (Online Updater). Given a target state, GeMuCo calculates the control input to realize the state and commands to the robot (Controller). Based on some sensors and actuators, the current latent state of the robot is calculated, and sensor values that cannot be directly obtained are estimated (State Estimator). Anomaly detection is performed based on the prediction errors of the sensor values (Anomaly Detector). GeMuCo can also be used to simulate the actual robot behavior based on the control input (Simulator).

A. Network Structure of GeMuCo

The network structure of GeMuCo is shown in the left figure of Fig. 2. First, we consider that there is a latent state z that can represent the current sensory and control inputs x . This means that when there exist, e.g. four kinds of sensory and control inputs $x = x_{\{1,2,3,4\}}$, all values of $x_{\{1,2,3,4\}}$ can be inferred by this z . Moreover, this z can be inferred using some or all of $x_{\{1,2,3,4\}}$. This means that each of the sensory and control inputs are correlated with each other via z . On the other hand, these relationships are difficult to handle as they are to construct a practical data structure of the model. Therefore, we expand this model and consider a model where the network inputs are $x_{\{1,2,3,4\}}$ and the mask variable m , the middle layer is the latent state z , and the network output is $x_{\{1,2,3,4\}}$. Here, we call the network from the input to the middle layer Encoder, and the network from the middle layer to the output Decoder. Let h denote

the function of the entire model, h_{enc} the function of the Encoder, and h_{dec} the function of the Decoder. Note that x is assumed to be normalized using all the data obtained.

1) **Mask Variable:** $m \in \{0, 1\}^{N_{sensor}}$ where N_{sensor} is the number of sensors and actuators) is a variable that masks the input $x_{\{1,2,3,4\}}$. If i -th line of m is 0, we set $x_i = 0$ and mask it completely. On the other hand, if x_i is 1, the current value x_i is used as network input. In other words, some of the inputs are masked by m , and z is computed from a limited number of network inputs. This makes it possible to infer the masked values and to use them for state estimation and anomaly detection. Of course, not all m is acceptable, and it is necessary to maintain a set of feasible masks \mathcal{M} . Note that the input and output of the network need not be the same. In this study, we represent the values used for the network input as x_{in} and the values used for the network output as x_{out} , and all the values used for the input/output of the network are expressed as x .

2) **Parametric Bias:** As a characteristic structure, p , parametric bias (PB) [25], is given as network input. This is a mechanism that has been mainly used in imitation learning and has been utilized in cognitive robotics research for the purpose of extracting multiple attractor dynamics from the obtained experience. The extraction of object dynamics from multimodal sensations [26] and the extraction of changes in hand-eye dynamics due to tool grasping [27] are being conducted. On the other hand, we do not directly use the parametric bias in the context of imitation learning in this study. We embed information on changes in the body, tools, and environment into this parametric bias, and update it according to the current state to adapt to the environment.

From the above, h , h_{enc} , and h_{dec} can be expressed as follows.

$$z = h_{enc}(x_{in}, m, p) \quad (1)$$

$$x_{out} = h_{dec}(z) \quad (2)$$

$$x_{out} = h(x_{in}, m, p) \quad (3)$$

B. Basic Usage of GeMuCo

The six basic usages (a)–(f) of GeMuCo and their application to the training and online update of GeMuCo and to the state estimation, control, and simulation using GeMuCo are

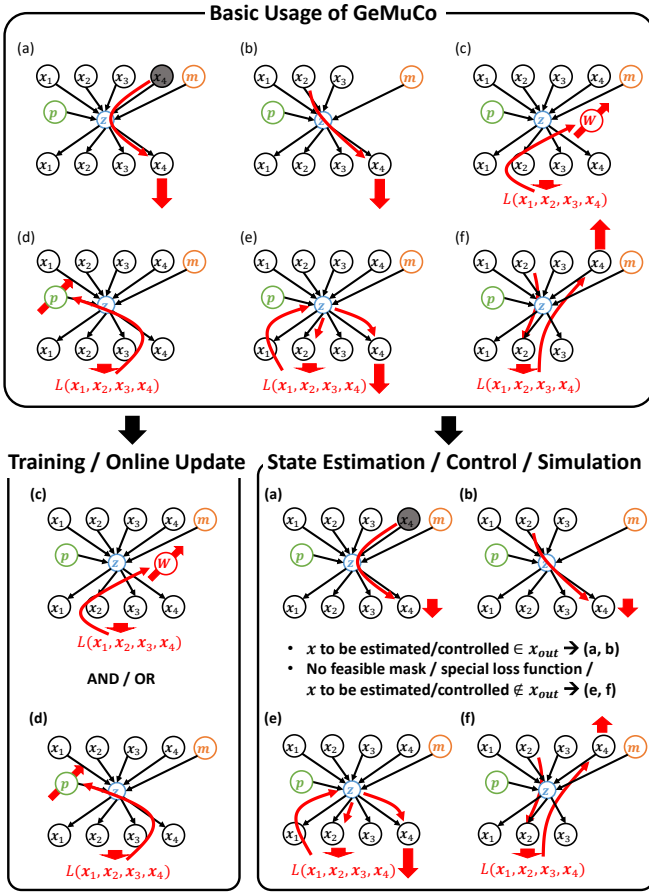


Fig. 3. The six basic usages of GeMuCo and their application to the training and online update of GeMuCo and to the state estimation, control, and simulation using GeMuCo. The six usages include the types of forward and backward propagations for network input/output, and (a)–(f) can be used in combination with each other. (a) estimates data that is currently unavailable. (b) is almost the same method as (a), but it is used when the output data to be inferred is not available in the input. (c) updates the network weight \mathbf{W} . (d) updates parametric bias \mathbf{p} . (e) estimates \mathbf{x}_{out} that optimizes a certain loss function by iterating forward and backward propagations. (f) is an iterative calculation similar to (e), but it corresponds to the case where the desired value is not available on the output side.

shown in Fig. 3. (a) and (b) relate to simple forward propagation, while (c)–(f) represent updates of values through repeated forward and backward propagations. Specifically, (c)–(f) comprehensively cover backpropagation with respect to network weight \mathbf{W} , parametric bias \mathbf{p} , latent space \mathbf{z} , and network input \mathbf{x}_{in} . Note that these are mere usages regarding the inference and updating of values, and when actually used in a robot, they should be employed in the form of Section II-F – Section II-K.

(a) is a method for estimating data that is currently unavailable. For example, if x_4 is not available, x_4 is inferred from $\mathbf{x}_{\{1,2,3\}}$ by setting \mathbf{m} to $(1 \ 1 \ 1 \ 0)^T$. In other words, the method masks the data that cannot be obtained and infers the data from the remaining data.

(b) is almost the same method as (a), but it is used when the output data to be inferred is not available in the input. For example, if x_4 needs to be obtained, it is inferred from $\mathbf{x}_{\{1,2,3\}}$

by setting \mathbf{m} to $(1 \ 1 \ 1)^T$. In other words, the method is the same as that of a normal neural network which infers data not in the input \mathbf{x}_{in} .

(c) corresponds to the adjustment of the network weight \mathbf{W} . A loss function L is defined with respect to the output, and the weight \mathbf{W} is updated from $\partial L / \partial \mathbf{W}$ as in general learning.

(d) corresponds to the adjustment of parametric bias \mathbf{p} . We define a loss function L with respect to the output and update \mathbf{p} from $\partial L / \partial \mathbf{p}$. While updating the weight \mathbf{W} changes the structure of the entire network, updating the parametric bias \mathbf{p} changes a part of the relationship and dynamics while preserving the overall structure of the network.

(e) is equivalent to computing \mathbf{x}_{out} that optimizes a certain loss function by iterating forward and backward propagations. First, \mathbf{z} is calculated by (a), (b), etc. Here, for example, if x_4 satisfying certain conditions needs to be computed, $\mathbf{x}_{\{1,2,3,4\}}$ is inferred from \mathbf{z} , the loss function is defined, and \mathbf{z} is updated from $\partial L / \partial \mathbf{z}$. By repeating this inference and update, x_4 with minimum loss function can be computed. In other words, the method minimizes the loss function by iterative inference and update on the decoder side.

(f) is an iterative calculation similar to (e), but it corresponds to the case where the desired value is not available on the output side. For example, if x_4 to be obtained is not in the output, the network output is inferred from $\mathbf{x}_{\{1,2,3,4\}}$, the loss function is defined, and x_4 is updated from $\partial L / \partial x_4$. By repeating this inference and update, x_4 can be computed such that the loss function is minimized. In other words, the method minimizes the loss function by iterative inference and update in the entire network, including Encoder and Decoder.

C. Data Collection for GeMuCo

In order to train GeMuCo, the necessary data of \mathbf{x} needs to be collected. There are two main methods: random action and human teaching. In random action, \mathbf{x} is obtained from random control inputs. It is also possible to consider a mapping from some random number to the control input, and use this mapping to operate the robot while applying constraints. In human teaching, a human directly decides the motion commands by using VR devices, sensor gloves, GUI applications, and so on. Data can be collected more efficiently for tasks that are difficult to perform by random action.

It is not necessary to collect data for all \mathbf{x} at all times. For example, it is acceptable if the robot vision is occasionally blocked, or if there are long intervals between some of the data collections. It is also acceptable to install a special sensor only when collecting data for training purposes. Also, \mathbf{x} to be collected is not necessarily limited to the information directly obtained from the robot’s sensors. It is possible to process the values of existing sensors before inputting them to the network, e.g. object recognition results obtained from image information or sound information related to specific frequencies, etc.

D. Training of GeMuCo

Although the training of GeMuCo described in this section is executed after the automatic determination of the network structure, it is explained first since it is necessary for the automatic structure determination as well.

When data D of \mathbf{x} is obtained, the output is usually inferred by taking \mathbf{x}_{in} as input and training GeMuCo so that it becomes close to \mathbf{x}_{out} using the mean squared error as the loss function. Here, it is necessary to include a mask variable \mathbf{m} in the training for GeMuCo. First, we prepare a set of feasible masks \mathcal{M} . Then, for each \mathbf{x}_{in} , we use each \mathbf{m} in \mathcal{M} to mask a part of the corresponding \mathbf{x}_{in} and create \mathbf{x}_{in}^{masked} . By inputting \mathbf{x}_{in}^{masked} and the corresponding \mathbf{m} , we train the weight \mathbf{W} of the network. In addition, \mathbf{x} is not always available for all the modalities. For example, there may be a situation where $\mathbf{x}_{\{1,2,4\}}$ is available but \mathbf{x}_3 is not. In this case, for the mask of \mathbf{x} , \mathbf{m} that can mask the data that cannot be obtained is chosen. If such \mathbf{m} is not included in \mathcal{M} , we do not train using this data. For the loss function, the mean squared error is calculated only for the obtained data, and the weight \mathbf{W} is updated.

In addition, when parametric bias \mathbf{p} is used as input, it is necessary to add one more step to the training method. In this case, we take data while changing the state of the body, tools, and environment. Let $D_k = \{\mathbf{x}_1, \mathbf{x}_2, \dots, \mathbf{x}_{T_k}\}$ ($1 \leq k \leq K$) where K is the total number of states and T_k is the number of data in the state k . Thus, the data used for training is $D = \{(D_1, \mathbf{p}_1), (D_2, \mathbf{p}_2), \dots, (D_K, \mathbf{p}_K)\}$. Here, \mathbf{p}_k is the parametric bias for the state k , which is a variable with a common value for the data D_k but a different value for different data. Using this data D , we simultaneously update the network weight \mathbf{W} and parametric bias \mathbf{p}_k . In other words, \mathbf{p}_k is introduced so that the data D_k of \mathbf{x} in each state k with different dynamics can be represented by a single network. This allows us to embed the dynamics of each state k into \mathbf{p}_k , which can be applied to state recognition and adaptation to the current environment. Note that \mathbf{p}_k is trained with an initial value of 0.

E. Automatic Structure Determination of GeMuCo

We describe a method for automatically determining the network structure of GeMuCo. Specifically, we determine \mathbf{x}_{in} , \mathbf{x}_{out} , and a set of feasible masks \mathcal{M} . If this network structure can be determined automatically from the given data, not only human work can be reduced, but also the autonomy of the robot can be dramatically improved. In other words, the robot can autonomously determine and train the network structure from the obtained data, and automatically construct state estimators, controllers, and so on based on the trained network structure. This operation mainly consists of determining network outputs that can be inferred from the latent space, and determining combinations of network inputs and masks that can infer the latent space, as shown in (a) of Fig. 4. Note that the number of layers and units of the network are given externally by humans, and these are not automatically determined (there are various mechanisms such as NAS for these [12]).

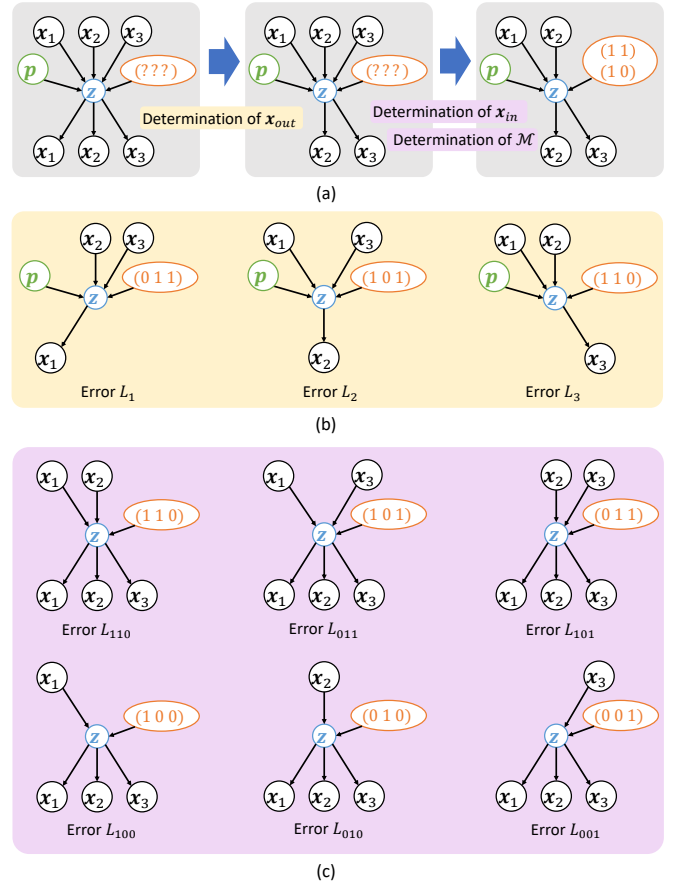


Fig. 4. (a) The overview of the automatic determination of network input/output of GeMuCo. (b) The loss definition to determine the network output \mathbf{x}_{out} of GeMuCo. (c) The loss definition to determine the network input \mathbf{x}_{in} and a set of feasible masks \mathcal{M} of GeMuCo.

1) **Network Training:** In order to determine \mathbf{x}_{in} , \mathbf{x}_{out} and a set of feasible masks \mathcal{M} , GeMuCo h is trained once using the obtained data D . The input/output of the network is determined based on the inference error when using the trained h . Here, in order to calculate the inference error for each mask \mathbf{m} , when training the network as in Section II-D, a set of all possible masks \mathcal{M}_{all} (all $2^{N_{sensor}} - 1$ combinations excluding masks that are all zero) is used. \mathbf{m} is randomly selected from \mathcal{M}_{all} each time.

2) **Determination of Network Output:** We determine the network output \mathbf{x}_{out} of GeMuCo. This can be judged from whether a given value \mathbf{x}_i is deducible from other values \mathbf{x}_j ($i \neq j$). If it is deducible, then \mathbf{x}_i is related to other sensors and actuators, and should be inferred as an output of the network. On the other hand, if it is not deducible, it should not be inferred because it will negatively influence the training of the network. As shown in (b) of Fig. 4, a value \mathbf{x}_i is inferred from other values \mathbf{x}_j and its inference error is L_i . We collect only \mathbf{x}_i for which $L_i < C_{thre}^{out}$, and construct \mathbf{x}_{out} using them. Sensor values not adopted here are not utilized as part of the network output.

3) **Determination of Network Input:** We determine the network input \mathbf{x}_{in} of GeMuCo. At the same time, we also

determine a set of feasible masks \mathcal{M} for the network input. This can be judged by the degree to which the value of \mathbf{x}_{out} determined in the previous procedure can be inferred from each mask. The masks that allow inference, i.e. the combinations of \mathbf{x}_i that allow inference, are extracted, and the set of such \mathbf{x}_i becomes \mathbf{x}_{in} . If all inference errors are large when using the mask \mathbf{m} containing a certain \mathbf{x}_i , then the \mathbf{x}_i should be removed from \mathbf{x}_{in} . First, we calculate the inference error L_m of \mathbf{x}_{out} for all \mathbf{m} . Let \mathcal{X}_{out} be the set of sensors included in \mathbf{x}_{out} . Here, it is obvious that \mathbf{x}_{out} can be inferred by the mask \mathbf{m} corresponding to the set of sensors \mathcal{X} such that $\mathcal{X}_{out} \subseteq \mathcal{X}$. Therefore, L_m is calculated only for the set of sensors \mathcal{X} such that $\mathcal{X}_{out} \not\subseteq \mathcal{X}$. For example, in (c) of Fig. 4, $\mathcal{X} = \{\mathbf{x}_1, \mathbf{x}_2, \mathbf{x}_3\}$ is excluded from the calculation process since $\mathcal{X}_{out} = \{\mathbf{x}_1, \mathbf{x}_2, \mathbf{x}_3\}$. We collect \mathbf{m} and the corresponding \mathbf{x}_i for which $L_m < C_{thre}^{in}$, and denote their union set as \mathcal{M} and \mathbf{x}_{in} , respectively.

The automatic network input/output determination of GeMuCo depends on the threshold values of C_{thre}^{out} and C_{thre}^{in} . Depending on the choice of these thresholds, the network structure changes, and the possible operations such as control and state estimation change accordingly. There is a tradeoff where setting low thresholds increase the accuracy of inference, but decrease the number of possible operations by reducing the number of input/output sensors. To mitigate this trade-off, there is a possibility of incorporating the accuracy of inference into the network by considering the output as both mean and variance. However, this aspect is not addressed in this study.

F. Online Update of GeMuCo

When the robot's physical state, tools, or surrounding environment changes, a model adapted to the current state can be used by updating GeMuCo for accurate state estimation and control. There are three possible ways to update the network: updating \mathbf{W} , updating \mathbf{p} , and updating \mathbf{W} and \mathbf{p} simultaneously. This corresponds to (c) and (d), or a combination of them in Fig. 3. When data D is obtained, the loss function is computed and the gradient descent method is used to update only \mathbf{W} , only \mathbf{p} , or \mathbf{W} and \mathbf{p} simultaneously. In the case of offline update, the network is updated once after a certain amount of data has been accumulated. In the case of online update, the network is updated gradually. When the number of data exceeds a determined threshold, data is discarded from the oldest. In addition to the actual D , if there are any constraints such as origin, geometric model, minimum and maximum values, etc., the data representing these constraints can also be added to D during the training. In the case of updating only \mathbf{p} , only some dynamics are changed and the structure of the overall network is kept the same, thus overfitting for the current data is unlikely to occur. On the other hand, it should be noted that updating \mathbf{W} or updating \mathbf{W} and \mathbf{p} simultaneously changes the structure of the entire network, and thus overfitting is likely to occur.

G. Optimization Computation by Iterative Forward and Backward Propagations

We describe the optimization computation that is frequently used in the state estimation, control, and simulation, which will be explained subsequently. This operation corresponds to (e) and (f) of Fig. 3, where the procedure of iterative optimization of \mathbf{x} or \mathbf{z} based on a certain loss function is shown. As an example, let us assume that \mathbf{z} is optimized based on the loss function for \mathbf{x}_{out} and that there is the relation $\mathbf{x}_{out} = \mathbf{h}_{dec}(\mathbf{z})$.

- 1) Assign the initial value \mathbf{z}^{init} to the variable \mathbf{z}^{opt} to be optimized
- 2) Infer the predicted value of \mathbf{x}_{out} as $\mathbf{x}_{out}^{pred} = \mathbf{h}_{dec}(\mathbf{z}^{opt})$
- 3) Calculate the loss L using the loss function \mathbf{h}_{loss}
- 4) Calculate $\partial L / \partial \mathbf{z}^{opt}$ using the backward propagation
- 5) Update \mathbf{z}^{opt} by gradient descent method
- 6) Repeat processes 2)–5) to optimize \mathbf{z}^{opt}

We now describe process 5) in detail. Process 5) performs the following operation,

$$\mathbf{z}^{opt} \leftarrow \mathbf{z}^{opt} - \gamma \frac{\partial L}{\partial \mathbf{z}^{opt}} \quad (4)$$

where γ is the learning rate. γ can be a constant, but we can also try various γ as variables to achieve faster convergence. For example, we determine the maximum value γ_{max} of γ , divide $[0, \gamma_{max}]$ equally into N_{batch} values (N_{batch} is a constant that expresses the batch size of training), and update \mathbf{z}^{opt} with each γ . Then, we select \mathbf{z}^{opt} with the smallest L in steps 2) and 3), and repeat steps 4) and 5) with various γ for the \mathbf{z}^{opt} .

H. State Estimation using GeMuCo

In state estimation, the sensor values that are currently unavailable are estimated from the network. For this purpose, (a), (b), (e), and (f) in Fig. 3 are used. If \mathbf{x}_{out} contains the value to be estimated, we consider the execution of (a) or (b), and if (a) and (b) are not possible, we consider the execution of (e). If \mathbf{x}_{out} does not contain the value to be estimated, we consider the execution of (f).

In (a), we consider a mask \mathbf{m} , which is set to 0 for the unavailable data and 1 for the available data. If this mask \mathbf{m} is included in the set of feasible masks \mathcal{M} , then by inputting this \mathbf{m} and \mathbf{x}_{in}^{masked} with $\mathbf{0}$ for the unavailable data into the network, we can estimate the currently unavailable data.

Similarly, in (b), if the network has all necessary inputs, the remaining data can be estimated directly. Even when the inputs are not available, if there exists a feasible \mathbf{m} , the missing data can be estimated in the same way as in (a).

If there is no feasible \mathbf{m} in the form of (a) and (b), state estimation is performed in the form of (e). This corresponds to the case where the loss function is set as follows in Section II-G,

$$\mathbf{h}_{loss}(\mathbf{x}_{out}^{pred}, \mathbf{x}_{out}^{data}) = \|\mathbf{m}_{x_{out}} \odot (\mathbf{x}_{out}^{pred} - \mathbf{x}_{out}^{data})\|_2 \quad (5)$$

where \mathbf{x}_{out}^{data} is the currently obtained data of \mathbf{x}_{out} with some unavailable data. Also, $\mathbf{m}_{x_{out}}$ is a mask that is 0 for unavailable data and 1 for available data. \odot denotes

Hadamard product, and $\|\cdot\|_2$ denotes L2 norm. In other words, this procedure corresponds to updating \mathbf{z}^{opt} so that the predictions are consistent only for the obtained data. The obtained \mathbf{x}_{out}^{pred} is used as the estimated state \mathbf{x}_{out}^{est} .

If \mathbf{x}_{out} does not contain the value to be estimated, state estimation is performed in the form (f). This corresponds to the case in Section II-G where the variable to be optimized \mathbf{z}^{opt} and its initial value \mathbf{z}^{init} are changed to \mathbf{x}_{in}^{opt} and \mathbf{x}_{in}^{init} , respectively. The loss function is the same as Eq. 5. That is, instead of the latent representation \mathbf{z} , we propagate the error directly to the network input \mathbf{x}_{in} and use the obtained \mathbf{x}_{in}^{opt} as the estimated state \mathbf{x}_{in}^{est} .

I. Control Using GeMuCo

Depending on the structure of the network, either (a), (b), (e), or (f) in Fig. 3 is computed, as in Section II-H. The calculation depends on whether the control input is contained in \mathbf{x}_{in} or \mathbf{x}_{out} , and whether the target state can be input directly or the target state needs to be expressed in the form of a loss function.

If the control input is contained in \mathbf{x}_{out} and all target states can be input directly from \mathbf{x}_{in} , then either (a) or (b) is performed. That is, $\mathbf{x}_{out} = \mathbf{h}(\mathbf{x}_{in}, \mathbf{m})$.

If the control input is contained in \mathbf{x}_{out} and the target state must be expressed in the form of a loss function, (e) is executed. This corresponds to the case where the loss function is executed in the form of $\mathbf{h}_{loss}(\mathbf{x}_{out}^{pred}, \mathbf{x}_{out}^{ref})$ in Section II-G. Here, \mathbf{x}_{out}^{ref} is the target state of \mathbf{x}_{out} , and \mathbf{h}_{loss} can take various forms, e.g. $\|A\mathbf{x}_1^{pred} - \mathbf{x}_1^{ref}\|_2$, $\|\mathbf{x}_1^{pred} - \mathbf{x}_1^{ref}\|_2 + \|\mathbf{x}_2^{pred}\|_2$, etc. ($\mathbf{x}_{\{1,2\}}^{(pred,ref)}$ represents the $\{1,2\}$ -th sensor value in $\mathbf{x}_{out}^{(pred,ref)}$), and A denotes a certain transformation matrix). \mathbf{z}^{opt} is optimized from this loss function, and the obtained \mathbf{x}_{out}^{pred} is used as the control input.

If the control input is not included in \mathbf{x}_{out} , (f) is executed. This means that the variable \mathbf{z}^{opt} to be optimized and its initial value \mathbf{z}^{init} in Section II-G are changed to \mathbf{x}_{in}^{opt} and \mathbf{x}_{in}^{init} , respectively. Since the loss function can also include the loss with respect to \mathbf{x}_{in}^{opt} , the loss function is $\mathbf{h}_{loss}(\mathbf{x}_{out}^{pred}, \mathbf{x}_{out}^{ref}, \mathbf{x}_{in}^{opt})$, unlike Eq. 5. In other words, the error is propagated directly to the network input \mathbf{x}_{in} instead of the latent representation \mathbf{z} . The obtained \mathbf{x}_{in}^{opt} is used as the control input.

J. Simulation using GeMuCo

In simulation, the current robot state is estimated from the control input and some constraints. The simulation can be performed in the form of (a), (b), (e), or (f), which is almost the same as the state estimation in Section II-H. The only difference is the loss functions in (e) and (f). Since the loss function does not have the current data \mathbf{x}_{out}^{data} as in the state estimation but instead has the control input value \mathbf{x}_{out}^{send} that is actually commanded, the loss function becomes $\mathbf{h}_{loss}(\mathbf{x}_{out}^{pred}, \mathbf{x}_{out}^{send})$. This loss function describes various constraints on the motion of the robot, such as joint torque, muscle tension, and motion speed. Based on the control input and the constraints given in the form of a loss function, the current state is estimated and transitioned.

K. Anomaly Detection using GeMuCo

Anomaly detection is performed with respect to the amount of error between the current value \mathbf{x}_{out} and the estimated value \mathbf{x}_{out}^{est} . One of the simplest anomaly detection methods is to set a threshold value for $\|\mathbf{x}_{out} - \mathbf{x}_{out}^{est}\|_2$ and consider an anomaly when the error is larger than the threshold. On the other hand, the mean and variance of the error can be used to detect anomalies more accurately. First, we collect the state estimation data \mathbf{x}_{out}^{est} and the current state data \mathbf{x}_{out}^{data} in the normal state without any anomaly. For this data, we calculate the mean $\boldsymbol{\mu}$ and variance $\boldsymbol{\Sigma}$ of the error $\mathbf{e}_{out}^{data} = \mathbf{x}_{out}^{data} - \mathbf{x}_{out}^{est}$. When actually detecting an anomaly, the difference \mathbf{e}_{out} between the current value \mathbf{x}_{out} and the estimated value \mathbf{x}_{out}^{est} is always obtained, and the Mahalanobis distance $d = \sqrt{(\mathbf{e}_{out} - \boldsymbol{\mu})^T \boldsymbol{\Sigma}^{-1} (\mathbf{e}_{out} - \boldsymbol{\mu})}$ is calculated for it. When d exceeds the threshold value, we assume that an anomaly has been detected.

III. EXPERIMENTS

In this study, we utilize the proposed body schema model of GeMuCo for (i) adaptive tool-tip control learning considering the change in grasping state, (ii) complex tendon-driven body control learning for musculoskeletal humanoids, and (iii) full-body tool manipulation learning for low-rigidity humanoids. (i) uses the simplest network structure, and due to its simplicity, no mask expression is required after the network structure is automatically determined. (ii) uses a more complex network structure but without parametric bias, in which the entire network is trained online. (iii) uses the most complex network structure, which contains all the elements of GeMuCo. These are newly interpreted experiments of [21]–[23] using the GeMuCo framework.

The reason for adopting each network structure is as below. When utilizing parametric bias, it is necessary to collect data while varying the state. Therefore, parametric bias is employed in cases where it is easy to vary the state, such as in (i) and (iii) scenarios involving changes in grasping state or tool conditions. On the other hand, for aspects such as correction of sim-to-real gap and body changes due to aging or deterioration, as in (ii), it is challenging to capture data while varying the state. Therefore, parametric bias is not used in such cases. Additionally, depending on the task, the collection of sensor values and the automatic determination of network input and output result in the determination of the network structure.

For the automatic determination of the network structure, $C_{thre}^{(out,in)}$ is generally set to $\{0.15, 0.15\}$. In (ii), we also analyze the case where $C_{thre}^{(out,in)} = \{0.3, 0.3\}$ in the sense of increasing the number of possible network operations.

A. Adaptive Tool-Tip Control Learning Considering Online Changes in Grasping State

Various studies have been conducted on tool manipulation, but they do not take into consideration the fact that the grasping position and angle of a tool changes gradually during tool manipulation. Moreover, few studies have dealt with deformable tools, and generally, only rigid tools fixed

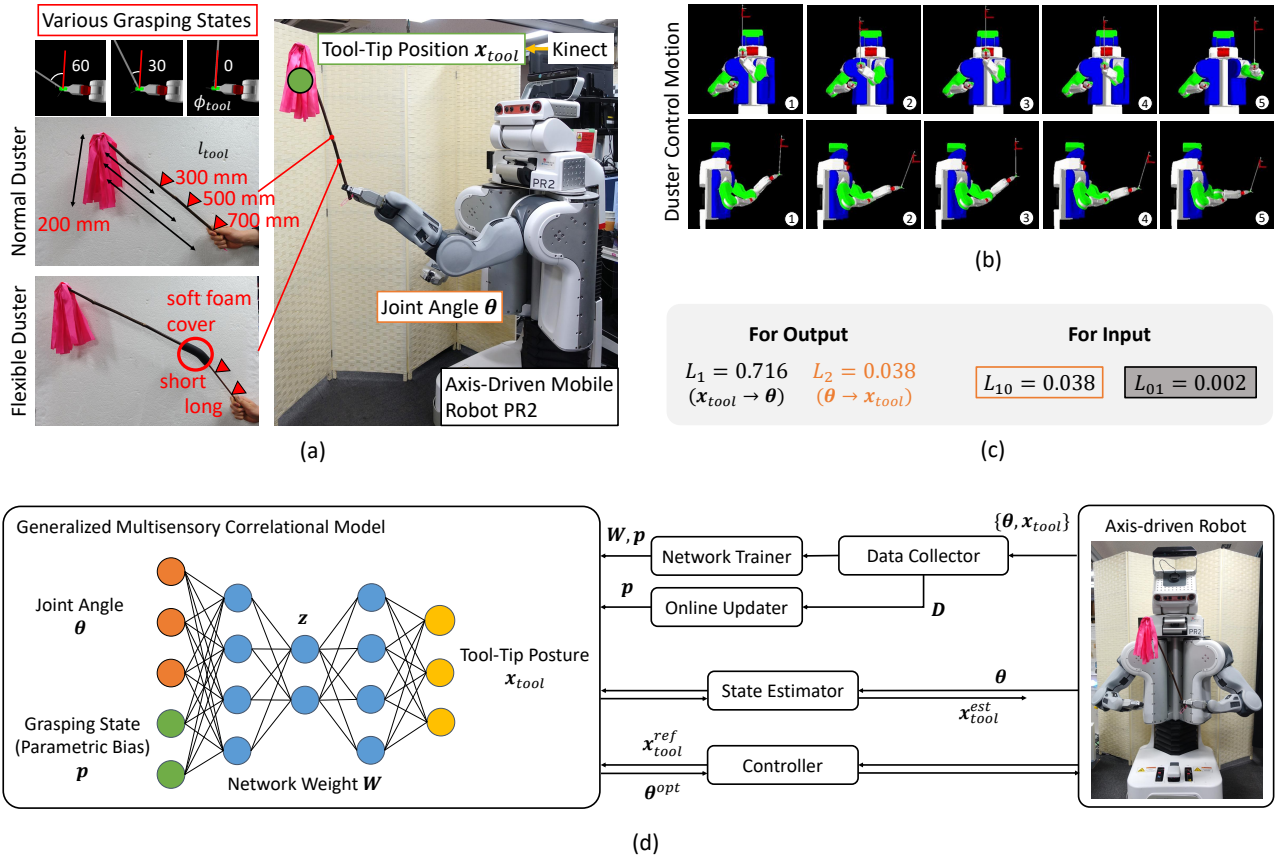


Fig. 5. (a) Adaptive tool-tip control learning considering online changes in grasping state. We prepared two types of dusters, Normal Duster and Flexible Duster, with various grasping states (grasping angle and position). The basic operation of dusters are shown in the bottom half. (b) The automatic determination of network structure for adaptive tool-tip control learning. (c) The system configuration for adaptive tool-tip control learning.

to the body have been considered. In this experiment, we propose a body schema learning method to control the tip position of rigid and flexible tools by considering gradual changes in the grasping state.

1) **Experimental Setup:** We conduct experiments using a duster as shown in (a) of Fig. 5. A duster is a tool to remove dust from shelves and crevices by controlling the tool-tip position. In this experiment, we set $x = \{x_{tool}, \theta\}$. Here, x_{tool} is the tool-tip position and θ is the 7-dimensional joint angle used as the control input to the robot.

Experiments using a simulation and the actual machine of the mobile robot PR2 are conducted. In the simulation experiment, we prepare an artificial cylinder (Normal Duster) to represent a duster. Since the cloth of the duster hangs down from the tip of the stick in the direction of gravity, the tool-tip position x_{tool} is assumed to be 100 mm below the tip of the stick in the simulation. The data is obtained by changing the grasping position of the duster (expressed as the length of the tool from the hand) l_{tool} and the grasping angle (angle perpendicular to the parallel gripper in one degree of freedom) ϕ_{tool} in three different ways: $l_{tool} = \{300, 500, 700\}$ [mm] and $\phi_{tool} = \{0, 30, 60\}$ [deg].

In the actual robot experiment, we handle a more difficult situation using a Flexible Duster, in which a Normal Duster and an additional stick are connected by a flexible foam

material, and the tool-tip position changes significantly depending on the angle at which the duster is held. The length of the duster used in the experiment is 500 mm, the length of the cloth is 200 mm, and the length of the additional stick is 250 mm. We perform Euclidean clustering of the color-extracted points of the cloth of the duster, and the center position of the largest cluster is the tool-tip position. As in the simulation experiment, l_{tool} and ϕ_{tool} are varied in the actual robot. Since the grasping state is implicitly trained even if the parameters of the grasping state are not directly known, the data is collected by manually and roughly creating grasping states with long/short tool length and $\phi_{tool} = \{0, 30, 60\}$.

Note that p is set to be two-dimensional in each experiment.

2) **Network Structure:** In the simulation, the joint angle is moved randomly, and 1000 data points per grasping state are collected, which amounts to 9000 data points in total. The automatic determination of the network structure based on the obtained data is shown in (c) of Fig. 5. First, we compute $L_{\{1,2\}}$ for determining the network output. While L_2 is small, L_1 is larger than C_{thre}^{out} and is not deducible. Therefore, the only output of the network is x_{tool} . Next, we compute L_m for determining the network input. Since the output is only x_{tool} , $L_{\{0,1,1\}}$ is not computed. Therefore, only L_{10} is computed, and as it is small enough (L_{10} is smaller than C_{thre}^{in}), the input

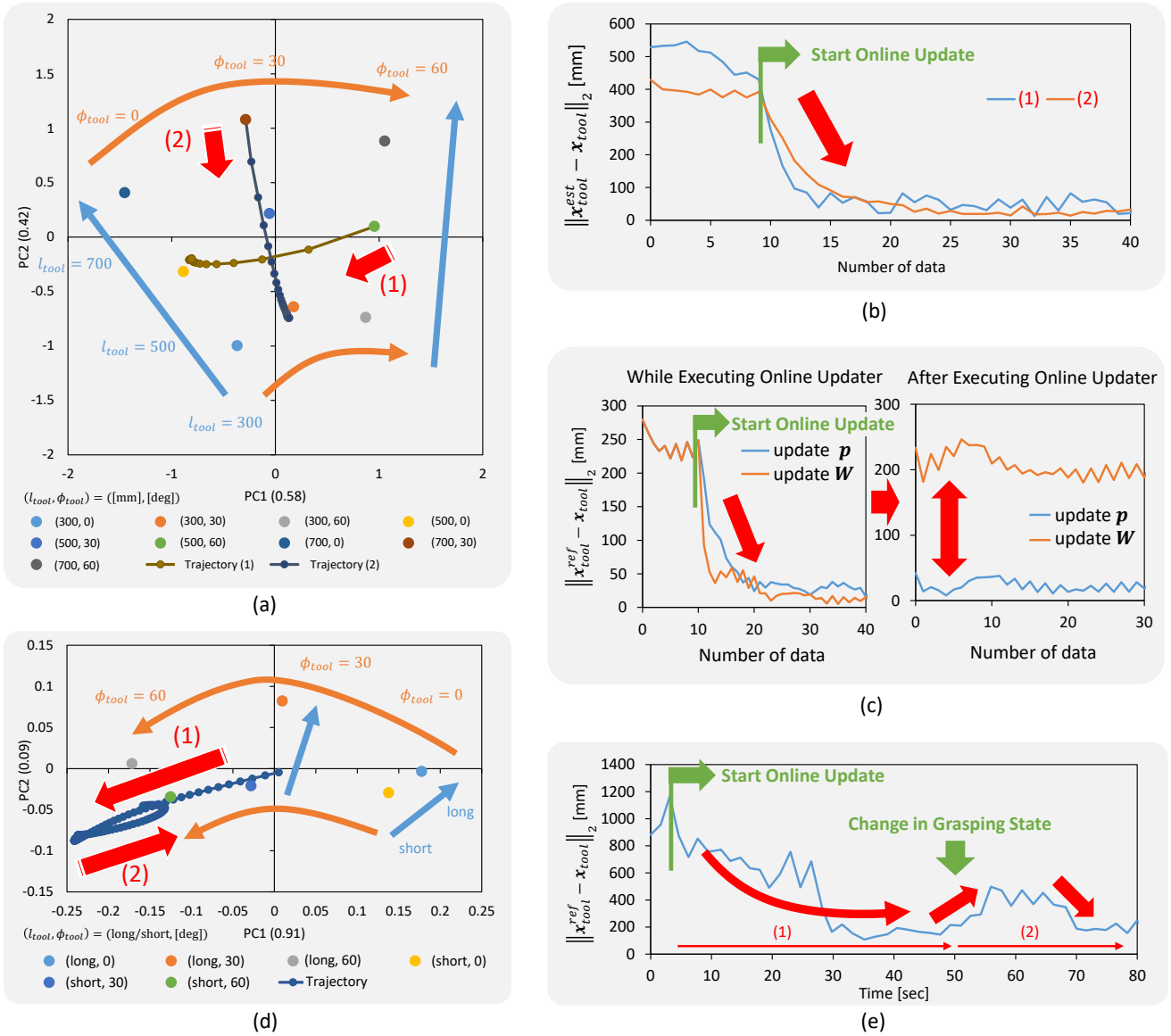


Fig. 6. (a) The trained parametric bias and its trajectory during online update of GeMuCo in the simulation experiment. (b) The transition of the state estimation error during online update of GeMuCo in the simulation experiment. (c) The transition of the control error while and after executing two types of online updaters, “update p ” and “update W ”, in the simulation experiment. (d) The trained parametric bias and its trajectory during online update of GeMuCo in the actual robot experiment. (e) The transition of the control error during online update of GeMuCo in the actual robot experiment [21].

is set to θ . The network $\theta \rightarrow x_{tool}$ is constructed and the system configuration shown in (d) of Fig. 5 is automatically constructed.

3) **Simulation Experiment:** First, we randomly move the joint angle in the simulation to obtain 1000 data points per grasping state, amounting to 9000 data points in total, and train the network based on these data points. The trained parametric bias p_k is represented in two-dimensional space through Principle Component Analysis (PCA) as shown in (a) of Fig. 6. We can see that each PB is neatly self-organized along the size of l_{tool} and ϕ_{tool} . The larger l_{tool} is, the larger the difference of PB with the change of ϕ_{tool} is, which is consistent with the point that the tool-tip position changes more significantly with the grasping angle for longer tools.

Next, we test the behavior of online update of parametric

bias and tool-tip position estimation. Experiments are performed for two cases in which the grasping state is changed from (1) $(l_{tool}, \phi_{tool}) = (500, 60)$ to $(l_{tool}, \phi_{tool}) = (500, 0)$ or (2) $(l_{tool}, \phi_{tool}) = (700, 30)$ to $(l_{tool}, \phi_{tool}) = (300, 30)$. The duster control motion is shown in (b) of Fig. 5 (with a tool at $(l_{tool}, \phi_{tool}) = (500, 30)$). The target tool-tip position x_{tool}^{ref} is repeatedly moved (200, -200) [mm] in the (x, z) direction and then moved back while advancing by 100 mm in the y direction from a certain reference point. The trajectories of parametric bias, “Trajectory (1)” and “Trajectory (2)”, during this duster motion are shown in (a) of Fig. 6, and the error of the estimated tool-tip position $\|x_{tool}^{est} - x_{tool}\|_2$ is shown in (b) of Fig. 6 (x_{tool}^{est} refers to the estimated value of the tool-tip position). For both (1) and (2), we can see that the parametric bias is gradually approaching the current grasping

state obtained at training phase. We can also see that the estimation error of the tool-tip position gradually decreases accordingly. The averaged estimation errors for (1) and (2) are 52.2 mm and 25.9 mm, respectively, when more than 20 data points were collected.

Finally, we experiment with the control of the tool-tip position. When the parametric bias is initially set to $(l_{tool}, \phi_{tool}) = (500, 30)$ obtained at training phase and then set to $(l_{tool}, \phi_{tool}) = (500, 60)$, we compare the control error when only \mathbf{p} is updated online (update \mathbf{p}) to when \mathbf{p} is fixed but \mathbf{W} is updated (update \mathbf{W}). The former case updates only \mathbf{p} , while the latter corresponds to updating the weight \mathbf{W} without \mathbf{p} , as in the usual online learning. The duster control motion is the same as in (b) of Fig. 5. Here, in order to use the joint angle θ^{orig} of (b) of Fig. 5 generated as $(l_{tool}, \phi_{tool}) = (500, 30)$, we set the loss as follows,

$$L = \|\mathbf{x}_{tool}^{pred} - \mathbf{x}_{tool}^{ref}\|_2 + 0.3\|\theta^{opt} - \theta^{orig}\|_2 \quad (6)$$

where \mathbf{x}_{tool}^{pred} is the predicted value of \mathbf{x}_{tool} and θ^{opt} is θ to be optimized. The transition of the control error of the tool-tip position $\|\mathbf{x}_{tool}^{ref} - \mathbf{x}_{tool}\|_2$ is shown in the left figure of (c) of Fig. 6. It can be seen that the control error is about 240 mm in the initial period when the online updater does not work, while the control error is significantly reduced by the online updater. When the number of data points obtained is more than 20, the average control error is 31.5 mm for “update \mathbf{p} ” and 19.2 mm for “update \mathbf{W} ”. The latter, which updates the entire network, is more accurate. The right figure of (c) of Fig. 6 shows the transition of the control error when the online updater is stopped and the same tool-tip position is realized by a different θ^{orig} with a different tool-tip rotation constraint. After updating only \mathbf{p} , the control error is 22.6 mm on average, while it is 207 mm after updating \mathbf{W} . It is found that the online update of grasping state is effective for other joint angles when only \mathbf{p} is updated, while the control error increases for other joint angles when \mathbf{W} is updated due to overfitting on the data used for training.

4) **Actual Robot Experiment:** The actual robot experiment is performed using PR2 with Flexible Duster. We perform the same operation with the simulation as shown in (b) of Fig. 5 three times while changing the reference point. We repeat the above motions while changing the grasping state, and train GeMuCo using the approximately 1500 data points that were obtained. At this time, the model obtained from the simulation described above is fine-tuned. The trained parametric bias is shown in (d) of Fig. 6. Since the Flexible Duster is more bendable than the Normal Duster, the parametric bias varies much more depending on the grasping angle than the grasping position (tool length).

The results of the tool-tip control experiment similar to the simulation experiment in (c) of Fig. 6 are shown in (e) of Fig. 6. The initial control error is very large (about 1000 mm), but the error is gradually reduced to about 150 mm as the current grasping state is recognized. When a human applies external force to the tool to change the grasping state, the control error increases to about 500 mm, but the error is reduced again to about 200 mm by online updater. The

transitions of PB are shown in “Trajectory” of (d) of Fig. 6, where (1) is the transition just after the start of online updater and (2) is the transition after the change of the grasping state. It can be seen that PB is autonomously updated by detecting the change of the grasping state.

B. Complex Tendon-driven Body Control Learning for Musculoskeletal Humanoids

We perform body schema learning that can handle state estimation, control, and simulation of musculoskeletal humanoids in a unified manner. By updating this network online based on the sensor data of the actual robot, the state estimation, control, and simulation of musculoskeletal humanoids can be performed more accurately and continuously. Note that the control is based on muscle length-based control, and dynamic factors including hysteresis due to high friction between muscles and bones are not handled in this experiment, resulting in handling only static relationships. In addition, since parametric bias is not used in this study, we do not obtain data for various body states.

1) **Experimental Setup:** In this experiment, we use a musculoskeletal humanoid Musashi [28] as shown in (a) of Fig. 7. We mainly use the 3 degrees of freedom (DOFs) of the shoulder and the 2 DOFs of the elbow as the joint angle θ . Ten muscles move the 5 DOFs of the shoulder and elbow, of which one muscle is a biarticular muscle. For each muscle, muscle length l is obtained from an encoder and muscle tension f from a loadcell. Although joint angle θ of musculoskeletal humanoids cannot be directly obtained because their joints are usually ball joints, Musashi can measure the joint angle with its pseudo-ball joint module [28]. Even if the joint angle cannot be directly measured, θ can be obtained by first estimating the rough joint angle based on muscle length changes and then correcting them using AR markers attached to the hand [29]. In this study, we set $\mathbf{x} = \{\theta, \mathbf{f}, \mathbf{l}\}$.

This musculoskeletal humanoid has a geometric model that is a representation of the muscle route by connecting the start, relay, and end points of the muscle with straight lines. Given a certain joint angle, muscle length can be obtained from the distance between the muscle relay points. By considering the elongation of the nonlinear elastic element attached to the muscle depending on muscle tension, the muscle length can be obtained from the given joint angle and the muscle tension. On the other hand, since it is difficult to simulate the wrapping of the muscle around the joint and its change over time, this geometric model is quite different from that of the actual robot and some learning using the actual robot sensor data is necessary.

2) **Network Structure:** We obtain 10000 data points from the random joint angle and muscle tension movements of the simulation. The automatic determination of the network structure based on the obtained data is shown in (b) of Fig. 7. First, $L_{\{1,2,3\}}$ is computed to determine the network output. While L_1 and L_3 are almost equally small, L_2 is somewhat larger. We now consider the cases where $0.247 < C_{thre}^{out} = 0.30$, i.e. all sensors are used for output, and where

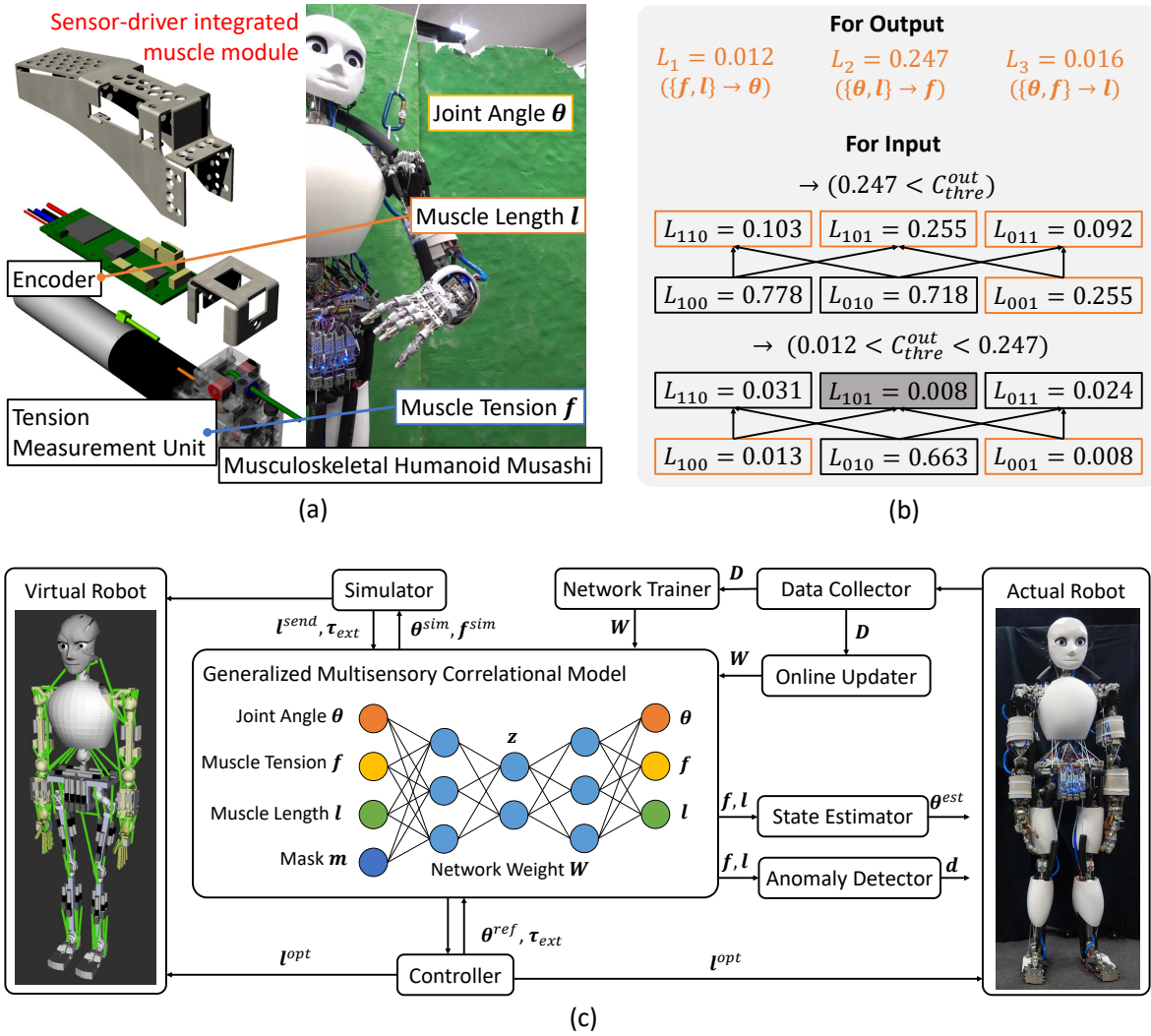


Fig. 7. (a) Complex tendon-driven body control learning for musculoskeletal humanoids with sensors of joint angle, muscle tension, and muscle length. (b) Automatic determination of network structure for complex tendon-driven body control learning. (c) The system configuration for complex tendon-driven body control learning.

$0.012 < C_{thre}^{out} = 0.15 < 0.247$, i.e. f is not used. For these cases, we compute L_m for network input determination. In the former case, when C_{thre}^{in} is set to 0.15, only L_{110} and L_{011} are less than this value, so (θ, f, l) , the union of sensors used in these masks, is used as the input (note that since the output is (θ, f, l) , L_{111} is not calculated). This is a network structure whose input and output are (θ, f, l) as well. When C_{thre}^{in} is set to 0.30, the number of mask types further increases from 2 to 4. In the latter case where f is not used for the output, when C_{thre}^{in} is set to about 0.015, only L_{100} and L_{001} are below this value, so (θ, l) , the union of the sensors used in these masks, is used as the input (note that since the output is (θ, l) , $L_{101,111}$ is not calculated). This is a type of network that does not take muscle tension into account. In other words, networks for various musculoskeletal structures can be constructed only with these different threshold values. In this study, we use the former network structure in which muscle tension is taken into account to enable various operations of GeMuCo. The

constructed system is shown in (c) of Fig. 7.

3) **Actual Robot Experiment:** First, we perform initial training of the network using a geometric model. The network is initialized from 10000 data points by obtaining muscle length from random joint angle and muscle tension movements. Next, we perform online update of the model based on the actual robot sensor data. Here, the online update is performed by repeatedly moving the robot with random joint angles and muscle tensions. The transition of the error between the estimated joint angle θ^{est} and the currently measured joint angle θ , $\|\theta^{est} - \theta\|_2$, is shown in (a) of Fig. 8. It can be seen that $\|\theta^{est} - \theta\|_2$ decreases gradually as the online update is executed. The exponential approximation of the results of the 10-minute experiment shows that the joint angle estimation error decreases from 0.324 rad to 0.154 rad in 10 minutes, which is about half of the original value.

We evaluate the state estimation using GeMuCo. We stopped the online updater after it was performed, and evaluated the joint angle estimation error before and after

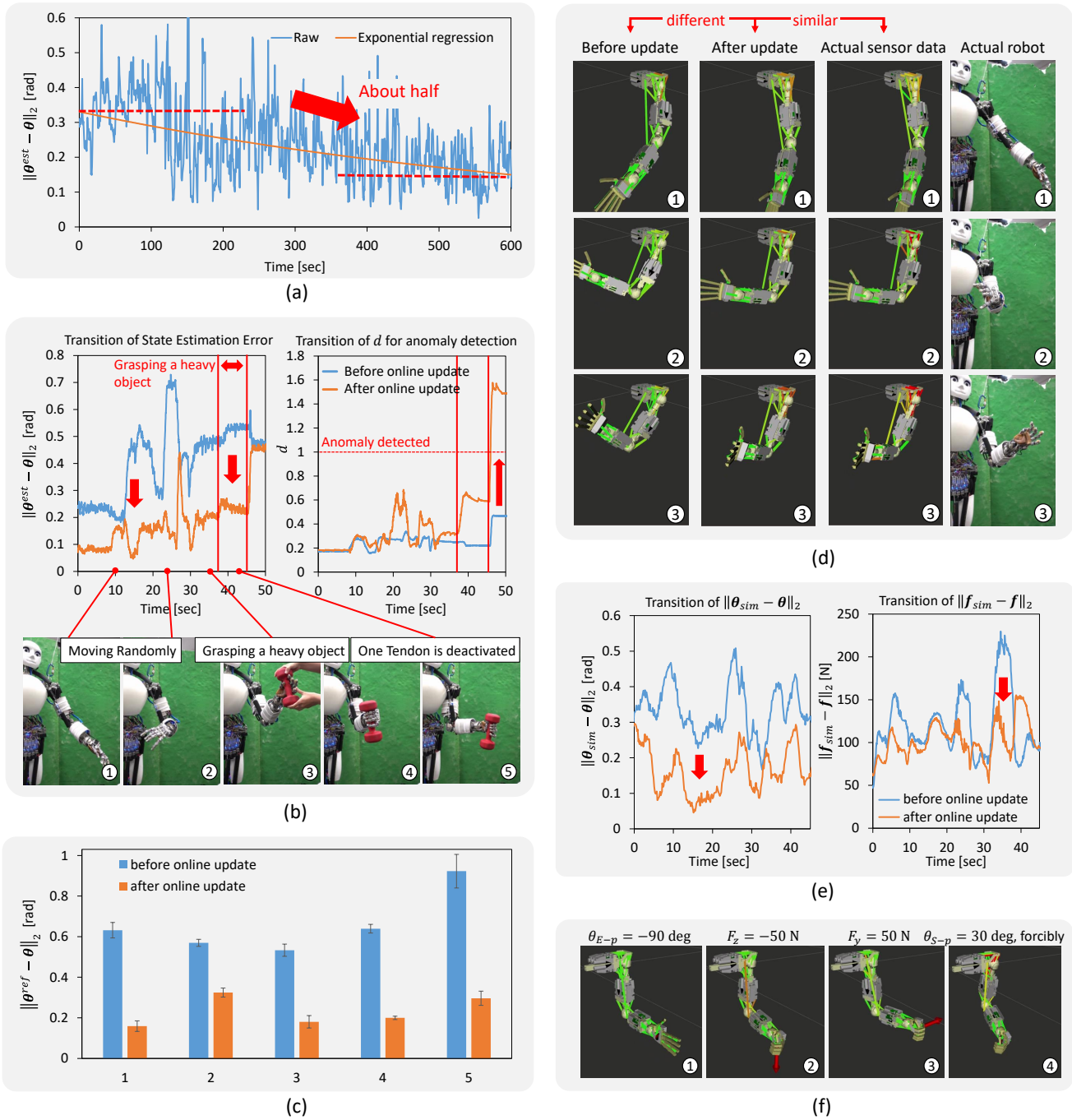


Fig. 8. (a) The transition of state estimation error while executing online updater. (b) The transition of state estimation error and anomaly score before and after online update of GeMuCo. (c) The control error before and after online update of GeMuCo. (d) The difference between the actual robot motion and the simulated robot motion before and after online update of GeMuCo. (e) The transition of the simulated joint angle and muscle tension errors before and after online update of GeMuCo. (f) Modification of the simulation behavior by changing the loss function [22].

the update. While the robot grasps a heavy object and then stops the function of one muscle, the joint angle estimation error and the anomaly d are measured. The experimental results are shown in (b) of Fig. 8. When the joints are moved randomly, the joint angle estimation error drops significantly from 0.414 rad to 0.186 rad on average after the online update. In addition, since the space of muscle tension is also learned during the online update, the joint angle estimation

error does not increase significantly even when a heavy object is grasped. After the online update, d rises sharply when stopping the function of one muscle, indicating that the robot can detect an anomaly. On the other hand, d does not rise much before the online update. This is because the muscle tension is determined randomly in the space as a whole during the initial training, so that the sensor values can be reconstructed even with infeasible muscle tension.

We evaluate the muscle length-based joint position control. The loss function is set as follows,

$$L = \|\boldsymbol{\theta}^{pred} - \boldsymbol{\theta}^{ref}\|_2 + \|\mathbf{f}^{pred}\|_2 + 0.01\|\boldsymbol{\tau}_{ext} + \mathbf{G}^T(\boldsymbol{\theta}^{ref}, \mathbf{f}^{pred})\mathbf{f}^{pred}\|_2 \quad (7)$$

where $\{\boldsymbol{\theta}, \mathbf{f}\}^{pred}$ is the predicted value from the network, $\boldsymbol{\theta}^{ref}$ is the target joint angle, \mathbf{G} is the muscle Jacobian obtained by differentiating the network, and $\boldsymbol{\tau}_{ext}$ is the desired joint torque (mainly gravity compensation torque). First, the target joint angle $\boldsymbol{\theta}^{ref}$ to be evaluated is randomly determined at five points. The motion from a random joint angle $\boldsymbol{\theta}_{rand}$ to $\boldsymbol{\theta}^{ref}$ is performed five times while changing $\boldsymbol{\theta}_{rand}$, and the average and variance of the control error $\|\boldsymbol{\theta}^{ref} - \boldsymbol{\theta}\|_2$ are evaluated. The results when using the model before and after the online update are shown in (c) of Fig. 8. It can be seen that the control after online update is more accurate in realizing the joint angle than that before the online update.

We evaluate the simulation constructed by GeMuCo. The loss function for the simulator is set as follows,

$$L = \|\mathbf{l}^{pred} - \mathbf{l}^{send}\|_2 + 0.1\|\mathbf{f}^{pred}\|_2 + 0.001\|\boldsymbol{\tau}_{ext} + \mathbf{G}^T(\boldsymbol{\theta}^{pred}, \mathbf{f}^{pred})\mathbf{f}^{pred}\|_2 \quad (8)$$

where \mathbf{l}^{send} refers to the muscle length commanded to the simulation and the calculated $\{\boldsymbol{\theta}, \mathbf{f}\}^{pred}$ is used as the simulated value $\{\boldsymbol{\theta}, \mathbf{f}\}^{sim}$. The comparison of sensor values during the simulation before and after online update and the actual robot motion is shown in (d) of Fig. 8. The higher the value of muscle tension, the redder the color of the muscle is, and the smaller the value of muscle tension, the greener the color is. It can be seen that the simulated muscle tension and joint angle are closer to the sensor values of the actual robot after the online update than before. Transitions of $\|\boldsymbol{\theta}^{sim} - \boldsymbol{\theta}\|_2$ and $\|\mathbf{f}^{sim} - \mathbf{f}\|_2$ before and after the online update are shown in (e) of Fig. 8. The average error between the actual sensor values and the simulated sensor values changes from 0.335 rad to 0.162 rad for the joint angles and from 104.8 N to 92.2 N for muscle tensions, which are smaller after the online update than before. This indicates that it is possible to make the behavior of the simulation closer to that of the actual robot by online update of GeMuCo. In addition, the simulation behavior can be modified by changing the loss function as shown in (f) of Fig. 8. This is the behavior when the elbow pitch angle θ_{E-p} is bent at 90 degrees, -50 N is applied in the z direction, 50 N in the y direction, and then the shoulder pitch angle θ_{S-p} is forced to 30 deg. The loss function of Eq. 8 is sufficient when specifying the force, but the loss function is set as the following when specifying the posture $\boldsymbol{\theta}_{fix}$ forcibly.

$$L = \|\mathbf{l}^{pred} - \mathbf{l}^{send}\|_2 + 0.1\|\mathbf{f}^{pred}\|_2 + \|\boldsymbol{\theta}^{pred} - \boldsymbol{\theta}_{fix}\|_2 \quad (9)$$

By changing the applied force or $\boldsymbol{\theta}_{fix}$, it is possible to check the corresponding changes in joint angle and muscle tension.

C. Full-Body Tool Manipulation Learning for Low-Rigidity Humanoids

In this experiment, a low-rigidity humanoid manipulates tools while maintaining balance with its body. Due to its low rigidity, the deflection of the body changes depending on the length and weight of the tool, and it is necessary to detect such changes while manipulating the tool.

1) **Experimental Setup:** In this experiment, KXR, a low-rigidity plastic-made humanoid, is used. We set $\mathbf{x} = \{\boldsymbol{\theta}, \mathbf{x}_{cog}, \mathbf{x}_{tool}, \mathbf{s}_{tool}\}$. Here $\boldsymbol{\theta} = (\theta_{S-p} \ \theta_{S-y} \ \theta_{E-p} \ \theta_{A-p})^T$ is the commanded joint angle (S for the shoulder, E for the elbow, A for the ankle, and py for the pitch and yaw, respectively). $\mathbf{x}_{cog} = (x_{cog} \ y_{cog})^T$ is the position of the center of gravity calculated from the single-axis force sensors placed at the four corners of each sole (since the position of the foot is not changed during tool manipulation, the feet are assumed to be aligned. z axis is ignored). \mathbf{x}_{tool} denotes the tool-tip position in the 3D space recognized by AR marker attached to the tool-tip. \mathbf{s}_{tool} denotes the tool-tip position in the 2D space in the image recognized by color extraction. If an AR marker is attached to the tool-tip, $\{\mathbf{x}_{tool}, \mathbf{s}_{tool}\}$ is obtained, while only \mathbf{s}_{tool} is obtained if there is no AR marker and only color extraction is executed. We attach the AR marker when collecting the training data, but this is removed when using the trained network because the AR marker is obstructive to tool manipulation.

In the experiments, we use a simulation and the actual robot of KXR. For both cases, we prepare tools with three different weights (Light: 40 g, Middle: 80 g, Heavy: 120 g) as shown in (a) of Fig. 9. In addition, we define two lengths (Short: 176 mm, Long: 236 mm) according to the grasped position of the tools, and handle a total of six tool states, which are combinations of these weights and lengths. (b) of Fig. 9 shows the changes in the tool-tip position and the center-of-gravity position when the actual KXR holds tools with different weights. For the same tool length, the tool-tip position differs by about 50 mm and the center of gravity by about 15 mm when holding a 40 g tool and a 120 g tool, due to the low rigidity of the hardware. Similarly, if the length of the tool changes, the tool-tip positions \mathbf{x}_{tool} and \mathbf{s}_{tool} change, and at the same time, the center of gravity \mathbf{x}_{cog} also changes. In order to simply reproduce the deflection of the actual robot in the simulation, each joint is simulated to be deflected by 30τ [deg] for the joint torque τ [Nm] applied to the body.

Note that \mathbf{p} is assumed to be two-dimensional in each experiment.

2) **Network Structure:** In the simulation, we randomly move the joint angle, and obtain 500 data points per one tool state, amounting to 3000 data points in total. The automatic determination of the network structure based on the obtained data is shown in (c) Fig. 9. First, L_i is computed and all values in \mathbf{x} are used as \mathbf{x}_{out} , since all are less than C_{thre}^{out} . Next, L_m is computed for each mask \mathbf{m} , and the feasible mask set is determined to be $\mathcal{M} = \{(1 \ 1 \ 1 \ 0)^T, (1 \ 1 \ 0 \ 1)^T, (1 \ 0 \ 1 \ 1)^T, (0 \ 1 \ 1 \ 1)^T, (1 \ 0 \ 1 \ 0)^T, (1 \ 1 \ 0 \ 0)^T\}$,

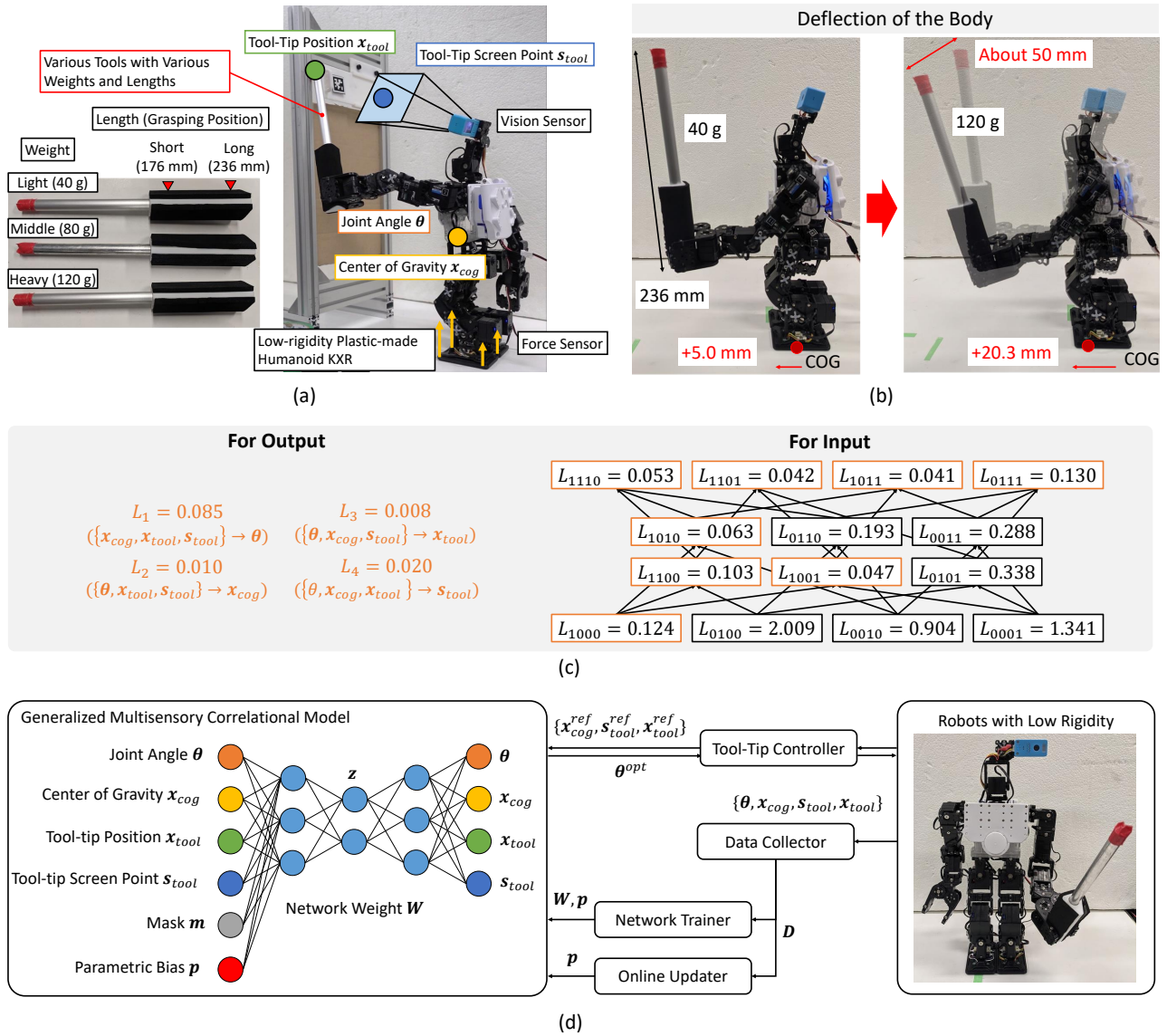


Fig. 9. (a) Full-body tool manipulation learning for low-rigidity humanoids with sensors of joint angle, center of gravity, tool-tip screen point, and tool-tip position. We prepared six types of tool states with various weights and lengths. (b) Due to the low rigidity of the hardware, the deflection of the body changes depending on the length and weight of the tool. (c) Automatic determination of the network structure for full-body tool manipulation learning. (d) The system configuration for full-body tool manipulation learning.

$(1 \ 0 \ 0 \ 1)^T, (1 \ 0 \ 0 \ 0)^T$. All values of x are used as x_{in} . The network $\{\theta, x_{cog}, x_{tool}, s_{tool}\} \rightarrow \{\theta, x_{cog}, x_{tool}, s_{tool}\}$ and the system configuration shown in (d) of Fig. 9 are automatically constructed.

3) **Simulation Experiment:** First, we randomly move the joint angle in the simulation, obtain 500 data per one tool state, amounting to 3000 data in total, and train the network based on these data. The trained parametric bias p_k is represented in two-dimensional space through PCA as shown in (a) of Fig. 10. We can see that each parametric bias is neatly self-organized along the weight and length of the tool.

Next, we show that the online update of parametric bias can make possible to accurately recognize the current tool state. We set the tools to the Long/Light and Short/Heavy

states and performed the online update of parametric bias while commanding random joint angles. The transitions of the parametric bias are shown in (a) of Fig. 10 (“long/light-traj” and “short/heavy-traj”). It can be seen that the current PB values are gradually approaching the Long/Light or Short/Heavy PB values obtained at training phase.

Next, we consider how the online update is affected by the different types of sensors used. If an AR maker is attached to the tool-tip, $\{x_{tool}, s_{tool}\}$ is obtained, while only s_{tool} is obtained if there is no AR marker and only color extraction is executed. Moreover, when the tool-tip is not within the sight of vision, we can only obtain $\{\theta, x_{cog}\}$. Therefore, in this experiment, there are three cases for the obtained data: A $\{\theta, x_{cog}\}$, B $\{\theta, x_{cog}, s_{tool}\}$, C $\{\theta, x_{cog}, x_{tool}, s_{tool}\}$, and we examine how the PB values transition in these three cases.

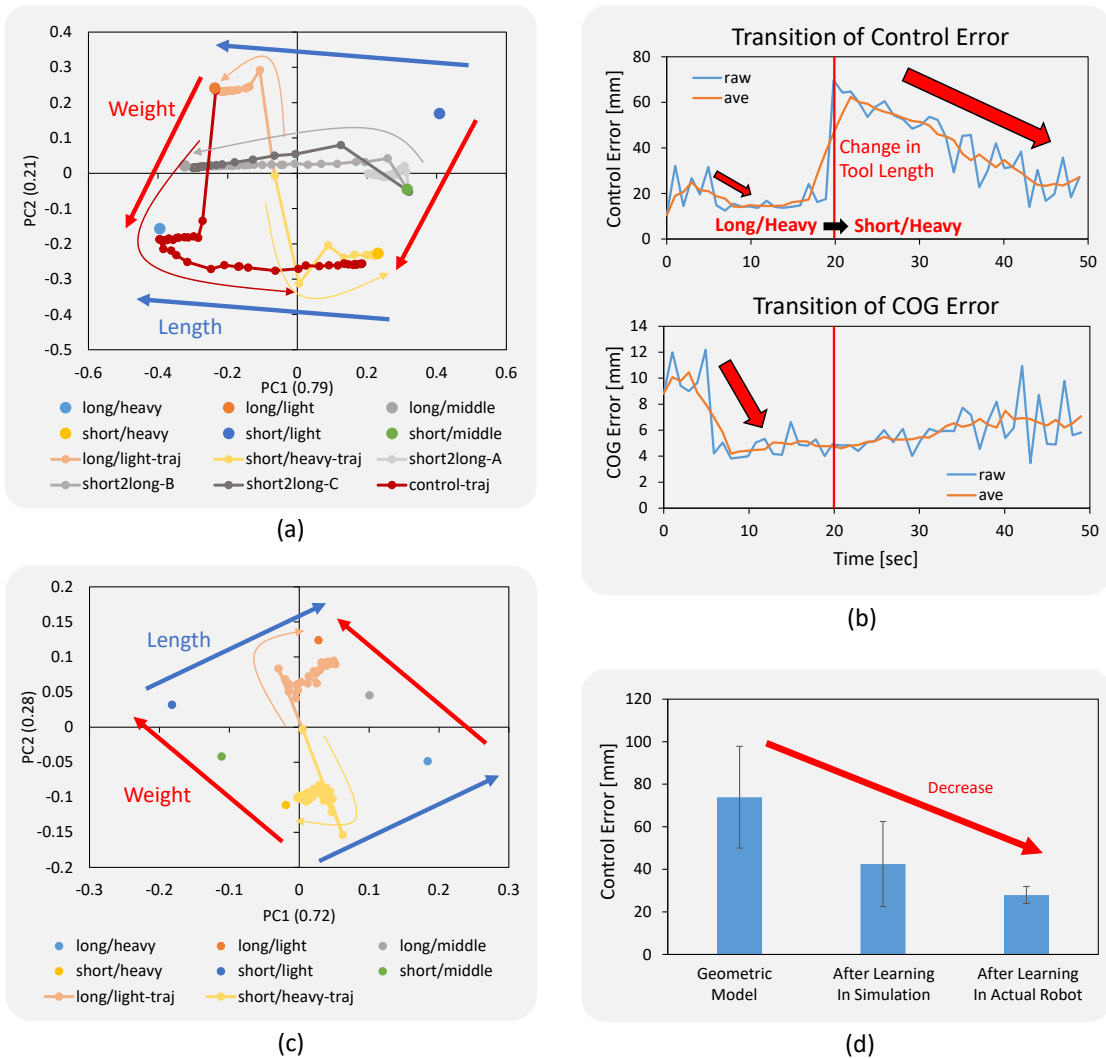


Fig. 10. (a) The trained parametric bias and its trajectory during online update of GeMuCo in the simulation experiment. (b) The transition of control and center-of-gravity errors in the simulation experiment. (c) The trained parametric bias and its trajectory during online update of GeMuCo in the actual robot experiment. (d) Comparison of control errors among when using a geometric model, using GeMuCo after training in simulation, and using GeMuCo after training in the actual robot [23].

Here, we start from the PB for Short/Middle obtained at the training phase and examine the case of grasping Long/Middle tools. The results are shown in (a) of Fig. 10 as “short2long-A”, “short2long-B”, and “short2long-C”. Case C has the same sensor type as the aforementioned “long/light-traj” and “short/heavy-traj”, and the PB transitions quickly in 15 steps, indicating that the tool state can be accurately recognized. In case B, the transition speed is slower than that of case C, and it takes 35 steps to accurately recognize the tool state. In case A, although PB is moving in the correct direction, it does not reach the correct value even after 35 steps of online update as in case B.

Finally, we conduct a control experiment including online update of parametric bias. We start from the state where the tool state is correctly recognized as Long/Light, and change the actual tool state in the order of Long/Heavy and Short/Heavy. The random target tool-tip position \mathbf{x}_{tool}^{ref} and the constant target center of gravity $\mathbf{x}_{cog}^{ref} = \begin{pmatrix} 0 & 0 \end{pmatrix}^T$ (coordinates

of the center of the foot) are given within the specified range, and GeMuCo is used to follow these target values. The loss function in this case is as follows.

$$L = \|\mathbf{x}_{tool}^{pred} - \mathbf{x}_{tool}^{ref}\|_2 + 0.01\|\mathbf{x}_{cog}^{pred} - \mathbf{x}_{cog}^{ref}\|_2 \quad (10)$$

The transition of parametric bias is shown in “control-traj” of (a) of Fig. 10. It can be seen that the parametric bias transitions from Long/Light to Long/Heavy to Short/Heavy, in order. The control error $\|\mathbf{x}_{tool}^{ref} - \mathbf{x}_{tool}\|_2$ and the center-of-gravity error $\|\mathbf{x}_{cog}^{ref} - \mathbf{x}_{cog}\|_2$ (raw) and each average of 5 steps (ave) are shown in (b) of Fig. 10. We can see that in the Long/Heavy condition, the control error is slightly decreased, and the center-of-gravity position error is significantly decreased by updating the PB value. It is because the tool state is changed from Long/Light to Long/Heavy and the weight of the tool changes significantly while the length of the tool remains the same. When the tool state is shifted to the Short/Heavy condition, the control error

changes significantly, but the center-of-gravity error does not change significantly. Similarly, the control error decreases significantly by online update of parametric bias.

4) **Actual Robot Experiment:** First, (1) data collection using a GUI (60 data points) and (2) data collection using random joint angles (20 data points) are performed for each tool, and a total of about 480 data points are collected. In (1), data is collected when a human directly specifies θ using a GUI. In (2), θ is specified randomly in the simulation, and is commanded to the actual robot when the center of gravity is within the support area and the tool-tip position is visible from the camera. By strengthening the constraint on the position of the center of gravity, it is possible to collect data to the extent that the robot does not fall over even if the simulation and the actual robot are different. Since the data obtained from the actual robot is limited, the model generated from the aforementioned simulation is fine-tuned. The arrangement of parametric bias obtained in this process is shown in (c) of Fig. 10. We can see that each parametric bias is neatly self-organized along the weight and length of the tool.

Next, we show that online update of this parametric bias can make it possible to accurately recognize the current tool state. We set the tools to Long/Light and Short/Heavy states, and perform online update of parametric bias while commanding random joint angles. The transition of the parametric bias is shown in (c) of Fig. 10 (“long/light-traj” and “short/heavy-traj”). It can be seen that the current PB values are gradually approaching the Long/Light and Short/Heavy PB values obtained at the training.

Finally, we evaluate the control error. (d) of Fig. 10 shows the comparison of the control errors at the Long/Middle tool state in the case of solving the full-body inverse kinematics using the geometric model, in the case of training GeMuCo from the simulation data including joint deflection, and in the case of fine-tuning GeMuCo using the actual robot sensor data. Note that the parametric bias when using GeMuCo is that of Long/Middle obtained at the training. It can be seen that the geometric model has the largest error, and the control error becomes smaller after training by simulation including joint deflection, and even smaller after training by the actual robot data.

IV. DISCUSSION AND LIMITATIONS

A. Discussion

First, in the tool-tip control experiment of PR2, we handled a very simple network configuration $\theta \rightarrow x_{tool}$. It is automatically detected that $\theta \rightarrow x_{tool}$ is computable, but the reverse is not. By collecting data in various grasping states, the information on the changes of these grasping states is embedded in parametric bias, and by updating it online, the current grasping state can always be recognized. In addition, the tool-tip position can be estimated and controlled based on the forward and backward propagation and gradient descent of the network, and these become more accurate when the grasping state is correctly recognized. Online update of parametric bias can maintain high generalization performance,

but updating the network weight W is prone to loss of generalization performance. Similarly, in the actual robot experiment with a flexible tool, online update of parametric bias and tool-tip control are possible, demonstrating the effectiveness of this system.

Next, in the body control experiment of the musculoskeletal humanoid Musashi, we handled a complex network configuration $(\theta, f, l) \rightarrow (\theta, f, l)$. There is a very complex relationship between $\{\theta, f, l\}$ in the musculoskeletal system, and in general there are three relationships: $\{\theta, f\} \rightarrow l$, $\{f, l\} \rightarrow \theta$, and $\{\theta, l\} \rightarrow f$. By expressing these relationships in a single network, state estimation, control, and simulation become possible. The network is initialized using data obtained from the geometric model and updated online using the actual robot sensor data. Unlike the aforementioned experiment, this is an example of updating W directly because it does not include parametric bias, but overfitting can be avoided by collecting data with random joint angles and muscle tensions. By updating the network with actual robot sensor data, the accuracy of state estimation, control, and simulation is improved. In terms of simulation, the proposed method can simulate various situations depending on the definition of the loss function, showing the versatility of the proposed method.

Finally, in the full-body tool manipulation experiment of the low-rigidity humanoid KXR, we handled an even more complex network configuration $\{\theta, x_{cog}, x_{tool}, s_{tool}\} \rightarrow \{\theta, x_{cog}, x_{tool}, s_{tool}\}$. Compared to the experiments in PR2, the addition of information on the center of gravity and the visual position of the tool enables a more diverse description of the loss function. By changing the weight and length of the tools, the tool information is embedded in the parametric bias as before, and this information can be correctly recognized from the changes in the center of gravity and the tool-tip position in the visual field. In particular, it was found that the more information available, the faster the online update of parametric bias converges, and the less information available, the longer it takes to recognize the tools. By controlling not only the tool-tip position but also the center-of-gravity position, it becomes possible for even a robot with low rigidity to perform stable tool manipulation. Also, by fine-tuning the simulation model with the actual robot data, more accurate tool manipulation control becomes possible.

B. Limitations

Based on these experimental results, we discuss the limitations and future prospects of this study.

First, data collection was generally performed by random action or human teaching using GUI. On the other hand, the concept of reinforcement learning is also effective in autonomously collecting valid data. We believe that the combination of this research with reinforcement learning will lead to a more practical system capable of generating complex motions.

Second, regarding catastrophic forgetting, updating only the low-dimensional latent space poses no problem when using parametric bias. However, updating the overall weight

W may lead to issues with catastrophic forgetting. Techniques such as Elastic Weight Consolidation [30] have been developed, and their incorporation should be considered in the future.

Third, regarding increasing sensor numbers, the current configuration results in an exponential increase in the number of masks based on sensor quantity, limiting the ability to infinitely add sensors. As the complexity of the body increases, the increase in sensor numbers becomes unavoidable, necessitating the development of more efficient learning methods.

Fourth, regarding anomaly detection, it is not possible to differentiate between anomalies and dynamic environmental changes. An anomaly is an unpredicted change, and to avoid categorizing an event as an anomaly, it is necessary to include observable sensor values for that event in the network input and output. However, the current setup only includes primitive sensors, and the incorporation of depth sensors, audio information, etc., will be necessary in the future.

Finally, to elevate the system to a more practical level, further application to diverse bodies, environments, tasks, and experiments is essential. Also, contributions to cognitive science and a deeper understanding of the relationship with the human brain are areas of interest for future research.

V. CONCLUSION

In this study, we have developed a method for robot control, state estimation, anomaly detection, simulation, and environmental adaptation by learning a body schema that describes the correlations between sensors and actuators of the robot's body, tools, and environment. By using a mask variable as input to the network, correlations between sensory and control input data can be described in the network. By using parametric bias, it is possible to incorporate the implicit changes in the correlation between body, tool, and environment into the model. By using the iterative backpropagation and gradient descent method, control, state estimation, anomaly detection, and simulation can be performed based on this single body schema. By updating the network weight and parametric bias, we can cope with changes in the grasping state of the object, changes in the characteristics of the tool, aging of the body, etc. With this method, we have succeeded in learning adaptive tool-tip control considering the changes in grasping state of an axis-driven robot, learning joint-muscle mapping for a musculoskeletal humanoid, and full-body tool manipulation considering tool changes for a low-rigidity plastic-made humanoid.

REFERENCES

- [1] P. Haggard and D. M. Wolpert, "Disorders of Body Scheme," in *Higher-Order Motor Disorders*, Ed. Freund, Jeannerod, Hallett, and Leiguarda. Oxford University Press, 2005.
- [2] M. Hoffmann, H. Marques, A. Arieta, H. Sumioka, M. Lungarella, and R. Pfeifer, "Body schema in robotics: a review," *IEEE Transactions on Autonomous Mental Development*, vol. 2, no. 4, pp. 304–324, 2010.
- [3] F. Zhang, J. Leitner, M. Jürgen, M. Milford, B. Upcroft, and C. Peter, "Towards vision-based deep reinforcement learning for robotic motion control," arXiv preprint arXiv:1511.03791, 2015.
- [4] S. Lathuilière, B. Massé, P. Mesejo, and R. Horaud, "Deep Reinforcement Learning for Audio-Visual Gaze Control," in *Proceedings of the 2018 IEEE/RSJ International Conference on Intelligent Robots and Systems*, 2018, pp. 1555–1562.
- [5] M. Zambelli, A. Cully, and Y. Demiris, "Multimodal representation models for prediction and control from partial information," *Robotics and Autonomous Systems*, vol. 123, p. 103312, 2020.
- [6] S. Levine, P. Pastor, A. Krizhevsky, J. Ibarz, and Q. J. et al., "Learning hand-eye coordination for robotic grasping with deep learning and large-scale data collection," *The International Journal of Robotics Research*, vol. 37, no. 4-5, pp. 421–436, 2018.
- [7] A. Krizhevsky, I. Sutskever, and G. E. Hinton, "Imagenet classification with deep convolutional neural networks," in *Proceedings of the 2012 Neural Information Processing Systems*, 2012, pp. 1097–1105.
- [8] D. Park, Y. Hoshi, and C. C. Kemp, "A Multimodal Anomaly Detector for Robot-Assisted Feeding Using an LSTM-Based Variational Autoencoder," *IEEE Robotics and Automation Letters*, vol. 3, no. 3, pp. 1544–1551, 2018.
- [9] C. Sun, W. He, and J. Hong, "Neural Network Control of a Flexible Robotic Manipulator Using the Lumped Spring-Mass Model," *IEEE Transactions on Systems, Man, and Cybernetics: Systems*, vol. 47, no. 8, pp. 1863–1874, 2017.
- [10] Y. Wu, K. Takahashi, H. Yamada, K. KIM, S. Murata, S. Sugano, and T. Ogata, "Dynamic Motion Generation by Flexible-Joint Robot based on Deep Learning using Images," in *Proceeding of the 8th Joint IEEE International Conference on Development and Learning on Epigenetic Robotics*, 2018.
- [11] H. V. Hoof, T. Hermans, G. Neumann, and J. Peters, "Learning robot in-hand manipulation with tactile features," in *Proceedings of the 2015 IEEE-RAS International Conference on Humanoid Robots*, 2015, pp. 121–127.
- [12] B. Zoph and Q. V. Le, "Neural architecture search with reinforcement learning," in *Proceedings of the 5th International Conference on Learning Representations*, 2017, pp. 1–16.
- [13] G. J. Bowden, G. C. Dandy, and H. R. Maier, "Input determination for neural network models in water resources applications. Part 1 - background and methodology," *Journal of Hydrology*, vol. 301, no. 1, pp. 75–92, 2005.
- [14] Y. Kobayashi, K. Harada, and K. Takagi, "Automatic controller generation based on dependency network of multi-modal sensor variables for musculoskeletal robotic arm," *Robotics and Autonomous Systems*, vol. 118, pp. 55–65, 2019.
- [15] J. Bongard, V. Zykov, and H. Lipson, "Resilient machines through continuous self-modeling," *Science*, vol. 314, no. 5802, pp. 1118–1121, 2006.
- [16] A. Cully and J. Clune and D. Tarapore and J. Mouret, "Robots that can adapt like animals," *Nature*, vol. 521, no. 7553, pp. 503–507, 2015.
- [17] M. Hoffmann, "Biologically inspired robot body models and self-calibration," in *Marcelo Ang; Oussama Khatib & Bruno Siciliano, ed., 'Encyclopedia of Robotics'*. Springer, 2022.
- [18] J. Hollerbach, W. Khalil, and M. Gautier, "Model identification," *Springer handbook of robotics*, pp. 113–138, 2016.
- [19] J. Sturm, C. Plagemann, and W. Burgard, "Body schema learning for robotic manipulators from visual self-perception," *Journal of Physiology-Paris*, vol. 103, no. 3, pp. 220–231, 2009.
- [20] D. Driess, F. Xia, M. S. Sajjadi, C. Lynch, A. Chowdhery, B. Ichter, A. Wahid, J. Tompson, Q. Vuong, T. Yu, et al., "PaLM-E: An Embodied Multimodal Language Model," in *Proceedings of the 40th International Conference on Machine Learning*, 2023, pp. 8469–8488.
- [21] K. Kawaharazuka, K. Okada, and M. Inaba, "Adaptive Robotic Tool-Tip Control Learning Considering Online Changes in Grasping State," *IEEE Robotics and Automation Letters*, vol. 6, no. 3, pp. 5992–5999, 2021.
- [22] K. Kawaharazuka, K. Tsuzuki, M. Onitsuka, Y. Asano, K. Okada, K. Kawasaki, and M. Inaba, "Musculoskeletal AutoEncoder: A Unified Online Acquisition Method of Intersensory Networks for State Estimation, Control, and Simulation of Musculoskeletal Humanoids," *IEEE Robotics and Automation Letters*, vol. 5, no. 2, pp. 2411–2418, 2020.
- [23] K. Kawaharazuka, K. Okada, and M. Inaba, "Adaptive Whole-body Robotic Tool-use Learning on Low-rigidity Plastic-made Humanoids Using Vision and Tactile Sensors," in *Proceedings of the 2024 IEEE International Conference on Robotics and Automation*, 2024.
- [24] K. Kawaharazuka, K. Okada, and M. Inaba, "Deep Predictive Model Learning with Parametric Bias: Handling Modeling Difficulties and

- Temporal Model Changes,” *IEEE Robotics Automation Magazine*, 2023.
- [25] J. Tani, “Self-organization of behavioral primitives as multiple attractor dynamics: a robot experiment,” in *Proceedings of the 2002 International Joint Conference on Neural Networks*, 2002, pp. 489–494.
- [26] T. Ogata, H. Ohba, J. Tani, K. Komatani, and H. G. Okuno, “Extracting multi-modal dynamics of objects using RNNPB,” in *Proceedings of the 2005 IEEE/RSJ International Conference on Intelligent Robots and Systems*, 2005, pp. 966–971.
- [27] S. Nishide, T. Nakagawa, T. Ogata, J. Tani, T. Takahashi, and H. G. Okuno, “Modeling tool-body assimilation using second-order Recurrent Neural Network,” in *Proceedings of the 2009 IEEE/RSJ International Conference on Intelligent Robots and Systems*, 2009, pp. 5376–5381.
- [28] K. Kawaharazuka, S. Makino, K. Tsuzuki, M. Onitsuka, Y. Nagamatsu, K. Shinjo, T. Makabe, Y. Asano, K. Okada, K. Kawasaki, and M. Inaba, “Component Modularized Design of Musculoskeletal Humanoid Platform Musashi to Investigate Learning Control Systems,” in *Proceedings of the 2019 IEEE/RSJ International Conference on Intelligent Robots and Systems*, 2019, pp. 7294–7301.
- [29] K. Kawaharazuka, S. Makino, M. Kawamura, Y. Asano, K. Okada, and M. Inaba, “Online Learning of Joint-Muscle Mapping using Vision in Tendon-driven Musculoskeletal Humanoids,” *IEEE Robotics and Automation Letters*, vol. 3, no. 2, pp. 772–779, 2018.
- [30] J. Kirkpatrick, R. Pascanu, N. Rabinowitz, J. Veness, G. Desjardins, A. A. Rusu, K. Milan, J. Quan, T. Ramalho, A. Grabska-Barwinska, et al., “Overcoming catastrophic forgetting in neural networks,” *Proceedings of the national academy of sciences*, vol. 114, no. 13, pp. 3521–3526, 2017.